Structural and Electrochemical Studies of Dimerization and Rotational Isomerization in Multi-Iron Silicotungstates

Travis M. Anderson,[a] Rui Cao,[a] Wade A. Neiwert,[a,c] Kenneth I. Hardcastle,[a] Craig L. Hill,*[a] Malika Ammam,[b] Bineta Keita,[b] and Louis Nadjo*[b]

Keywords: Polyoxometalates / Cyclic voltammetry / Iron / Tungsten

A structural and electrochemical investigation of dimerization and Baker–Figgis (rotational) isomerization in the tri-ferric-substituted silicotungstates has been undertaken because these phenomena are important in a large number of polyoxometalates. A single-crystal X-ray diffraction analysis of $K_4Na_7[(\beta\text{-}SiFe_3W_9(OH)_3O_{34})_2(OH)_3]$ (**β1**) has been carried out [a = 12.9709(7) Å, b = 38.720(2) Å, c = 21.4221(12) Å, orthorhombic, *Pbcm*, R_1 = 8.48 %, based on 13809 independent reflections]. The complex is isostructural with $[(\alpha\text{-}SiFe_3W_9(OH)_3O_{34})_2(OH)_3]^{11-}$ (**α1**) except that the edge-shared W_3O_{13} caps in each $[SiFe_3W_9(OH)_3O_{34}]^{4-}$ unit are rotated by 60°. Electrochemical measurements, performed in a pH 5 acetate buffer, indicate a positive shift in the Fe^{III}-based peak potential (and no change for the W^{VI}-based potential) upon going from **α1** to its monomeric derivative $[(\alpha\text{-}Si(FeOH_2)_3W_9(OH)_3O_{34})]^{4-}$ (**α2**) (–0.484 ± 0.005 V and –0.474 ± 0.005 V, respectively). In contrast, the peak potentials of the Fe^{III}- and W^{VI}-based redox processes of **β1** are both found at more negative values than its rotational isomer **α1**. The absolute values of the reduction peak potential differences are 0.022 V for Fe^{III} and 0.162 V for W^{VI}.

Introduction

The use of polyoxometalates (POMs) as catalysts constitutes a substantial and rapidly growing literature.[1,2] In particular, d-electron-transition-metal-substituted POMs have attracted much attention as oxidation catalysts because they are thermodynamically stable to oxidative degradation; yet many of the fundamental properties of POMs that impact catalysis and other applications as well, including elemental composition, solubility, redox potentials, charge density, size, and shape, can be systematically altered to a considerable degree. As a result, these compounds combine the stability advantages of heterogeneous catalysts with the selectivity advantages of homogeneous catalysts.

Recently we began a program aimed at the synthesis and characterization of a series of multi-iron heteropolytungstates with the goal of exploring their redox chemistry and catalytic (and electrocatalytic) properties.[3] In general, parameters (such as pH and heteroatom effects) that favor multi-electron-transfer reactions in POMs continue to be a focus on ongoing efforts.[4,5] Previously it was shown in a comparison of the cyclic voltammograms of α_1- and α_2-$[P_2(FeOH_2)W_{17}O_{61}]^{7-}$ that the location of Fe^{III} (cap or belt site) within the heteropolytungstate framework influences the electrochemical properties of the molecules.[6] More recently, we have also shown that the accumulation of multiple edge-sharing Fe^{III} centers in Wells–Dawson-derived sandwich-type complexes leads to more favorable electrocatalytic properties than those observed in monosubstituted complexes such as α_2-$[As(FeOH_2)W_{17}O_{61}]^{7-}$.[7]

This paper focuses on how two different types of common POM structural perturbations influence the electrochemical properties of Fe^{III} redox centers in a series of multi-iron silicotungstates (Figure 1). In one study, two complexes differing only in the rotational arrangement (i.e. Baker–Figgis isomerism)[8] of their edge-shared W_3O_{13} caps, $[(\alpha\text{-}SiFe_3W_9(OH)_3O_{34})_2(OH)_3]^{11-}$ (**α1**) and $[(\beta\text{-}SiFe_3W_9(OH)_3O_{34})_2(OH)_3]^{11-}$ (**β1**), are compared. In the other study, the dimer, **α1**, is compared with its monomeric analogue, $[(\alpha\text{-}Si(FeOH_2)_3W_9(OH)_3O_{34})]^{4-}$ (**α2**).[9] Unlike **α1** and **β1**, complexes **α1** and **α2** have different coordination environments around their Fe^{III} centers. The replacement of a hydroxo ligand in **α1** with an aqua ligand in **α2** results in a 20-nm red shift (from 436 nm to 456 nm) for the Fe^{III}-centered d-d transitions in the electronic spectra of the two complexes.

[a] Department of Chemistry, Emory University, Atlanta, Georgia 30322, USA
E-mail: chill@emory.edu
[b] Laboratoire de Chimie Physique, UMR 8000, CNRS, Université Paris-Sud, Bâtiment 420, 91405 Orsay Cedex, France
E-mail: nadjo@lcp.u-psud.fr
[c] Current address: Department of Chemistry, Bethel University, St. Paul, Minnesota 55112, USA
Supporting information for this article is available on the WWW under http://www.eurjic.org or from the author.

  DOI: 10.1002/ejic.200401061

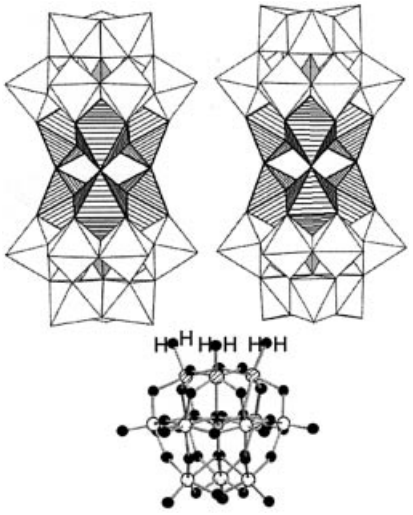

Figure 1. Polyhedral representations of $[(\alpha\text{-}SiFe_3W_9(OH)_3O_{34})_2(OH)_3]^{11-}$ (**α1**, top left) and $[(\beta\text{-}SiFe_3W_9(OH)_3O_{34})_2(OH)_3]^{11-}$ (**β1**, top right), and a ball-and-stick representation of $[(\alpha\text{-}Si(FeOH_2)_3W_9(OH)_3O_{34})]^{4-}$ (**α2**, bottom). White, gray, and striped polyhedra represent WO_6, SiO_4, and FeO_6, respectively (**α1** and **β1**). In **α2**, the W, Fe, Si, and O atoms are shown as white, striped, gray, and black spheres, respectively.

Results and Discussion

Syntheses: The syntheses of $[\alpha\text{-}SiFe_3W_9(OH)_3O_{34}]^{4-}$ (**α2**) and $[\beta\text{-}SiFe_3W_9(OH)_3O_{34}]^{4-}$ (**β2**) were originally reported by Pope.[10] However, mass spectrometry data suggested these complexes contained small to modest amounts of the dimeric species ($[(\alpha\text{-}SiFe_3W_9(OH)_3O_{34})_2(OH)_3]^{11-}$ (**α1**) and $[(\beta\text{-}SiFe_3W_9(OH)_3O_{34})_2(OH)_3]^{11-}$ (**β1**), respectively) as impurities.[10] Recently, we reported a modified procedure that utilizes differences in the acid sensitivities of $Na_7H_3[\alpha\text{-}SiW_9O_{34}]$ and $K_{10}[\alpha\text{-}SiW_9O_{34}]$ to obtain **α1** and **α2**, respectively, in high purity (with 40–70% yield).[9] In this report, an analogous procedure is used to obtain **β1** (i.e. reaction of $Na_9H[\beta\text{-}SiW_9O_{34}]$ with 3 equivalents of Fe^{III} in 0.5 M sodium acetate (pH = 6) yields **β1** in 20% yield).

Solid State Characterization of β1: The X-ray crystallographic studies of **β1** show that two A-type $[\beta\text{-}SiFe_3W_9(OH)_3O_{34}]^{4-}$ units are linked by three Fe-μ-OH–Fe bridges such that the complex has overall ca. D_{3h} symmetry (Figure 1). The complex is isostructural with **α1** except that the edge-shared W_3O_{13} caps in each $[SiFe_3W_9(OH)_3O_{34}]^{4-}$ unit are rotated by 60°. Table 1 gives average bond lengths and angles for the two complexes. Bond valence sum (BVS) calculations for Fe1, Fe2, Fe3, and Fe4 (see Figure S1 in the Supporting Information for the numbering scheme; for supporting information see also the footnote on the first page of this article) give average oxidation states of 2.96, 2.99, 3.06, and 2.99, respectively.[11] BVS calculations (average value = 1.2) also establish that hydroxo bridges are present between the adjacent Fe^{III} centers in each $[SiFe_3W_9(OH)_3O_{34}]^{4-}$ unit.

Table 1. Selected average bond lengths [Å] and bond angles [°] for **α1** and **β1**.

	α1[a]	**β1**
W=O	1.724(8)	1.718(8)
Si–O	1.64(1)	1.63(3)
Fe···Fe	3.713(8)	3.710(11)
W_{belt}–O–W_{cap}	150.4(5)	145.7(8)
Fe1···Fe2···Fe3	61.0(3)	59.1
W1···W2···W3	59.9(3)	60.4

[a] Data from reference[9].

The differential scanning calorimetry curve for **β1** shows one endothermic and two exothermic processes in the region from 20 °C to 600 °C (Figure 2). The endothermic process from 100 °C to 160 °C is attributed to desorption of water molecules of crystallization from the lattice structure. This conclusion is corroborated by thermogravimetric analysis and infrared spectroscopy. The first exothermic process (from 200 °C to 275 °C, indicated by arrows and verified by infrared data) is attributed to the solid-state isomerization (from **β1** to **α1**) of the POM. Infrared spectroscopy shows that there is an 18 cm^{-1} shift in the combination W=O stretching/W–O–W bending mode centered at 883 cm^{-1} in **β1** upon heating the sample to 275 °C. The 18 cm^{-1} shift places this band at 901 cm^{-1}, which is identical to that reported for an authentic sample of **α1** (Figure 3).[9] Finally, there is an exothermic process observed from 550 °C to 600 °C that is attributable to the collapse of the tungsten framework of the POM. This is also corroborated by infrared spectroscopy data, which shows significant changes in the W=O (W–O) stretching and W–O–W bending modes after heating to 550 °C.

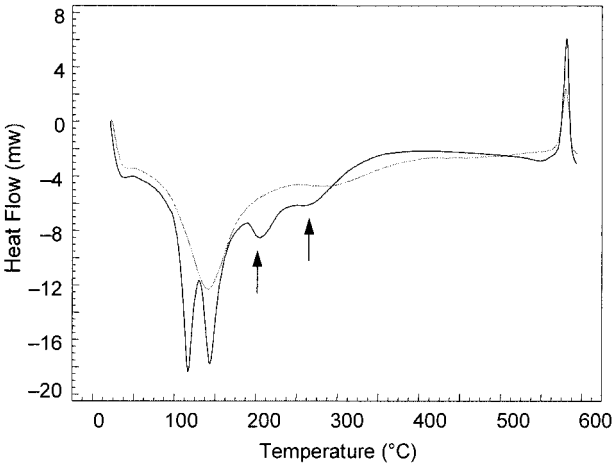

Figure 2. Differential scanning calorimetry data for $K_4Na_7[(\beta\text{-}SiFe_3W_9(OH)_3O_{34})_2(OH)_3]$ (**β1**) (black line) and $K_4Na_7[(\alpha\text{-}SiFe_3W_9(OH)_3O_{34})_2(OH)_3]$ (**α1**) (gray line). The endothermic desorption of solvent water molecules of crystallization from 100 °C to 160 °C in **β1** is nearly resolved into two peaks, whereas the same process in **α1** appears as only one broad peak. The arrows are used to indicate the temperature range of the first exothermic feature based on infrared data. This corresponds to where the solid state rotational isomerization of the W_3O_{13} caps takes place.

Electrochemical Studies: Recently, we reported the detailed electrochemical behavior of the Fe^{III} centers within a

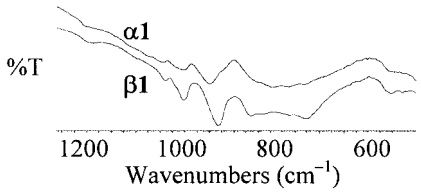

Figure 3. Infrared spectra of **α1** (top) and **β1** (bottom). The spectra are shown in percent transmittance (and labeled as %T on the *y* axis). The band at 883 cm^{-1} in the spectrum of **β1** is shifted by 18 cm^{-1} (to 901 cm^{-1}) in **α1**.

large family of related sandwich-type complexes, including αββα-$[(Fe^{III}OH_2)_2(Fe^{III})_2(X_2W_{15}O_{56})_2]^{12-}$ (X = P^V or As^V).[3a,4,7] In a pH 5 acetate buffer, these compounds show a stepwise reduction of the four edge-sharing Fe^{III} centers. In contrast, the corner-sharing Fe^{III} centers in **α1**, **α2**, and **β1** have a single Fe^{III}-based voltammetric wave in the same pH 5 acetate buffer. In addition, unlike the sandwich-type complexes, **α1**, **α2**, and **β1** also adsorb to different extents onto the surface of the glassy carbon electrode. This behavior was discovered by the observation that there is a steady negative shift in the potentials of the complexes in every other run. This phenomenon is slight for complexes **α1** and **α2**, but it is more pronounced for **β1**. All of the electrochemical data presented in the following paragraphs were obtained with freshly polished glassy carbon electrodes except where noted.

Figure 4 (A) shows the cyclic voltammogram of **α1** in the pH 5 acetate buffer with a scan rate of 10 mV·s^{-1}. The pattern has been restricted to the reduction of the Fe^{III} centers and the first W^{VI} reduction process. The W^{VI}-based wave is electrochemically quasi-reversible and chemically reversible upon reversal of the potential. The Fe^{III}-based wave in this system is observed at E_{pc} = –0.484 ± 0.005 V (vs. SCE). Controlled potential coulometry experiments (with the potential set at –0.550 V vs. SCE) indicate that **α1** consumes 6.08 ± 0.05 electrons per molecule. This is consistent with the simultaneous one-electron reduction of the six Fe^{III} centers. The characteristic blue color of a reduced tungsten-oxygen framework was not observed during this experiment, consistent with the observation that there is a large separation between the Fe^{III}- and the W^{VI}-based redox processes. Finally, it was possible to completely re-oxidize **α1** back to the Fe^{III} state, which confirms and also extends the time dependence of the chemical reversibility and stability of the complex previously observed by cyclic voltammetry.

Figure 4 (B) compares the cyclic voltammograms of **α1** and **α2** under identical conditions (0.2 mM POM in 0.5 M acetate buffer, pH 5; scan rate 10 mV·s^{-1}). The Fe^{III}-based waves of the two complexes have slightly different shapes, with **α2** showing a larger half peak width than **α1** (0.118 vs. 0.080 V for **α2** and **α1**, respectively). The peak potential of **α2** is also at a more positive value than **α1** (–0.474 ± 0.005 V vs. –0.484 ± 0.005 V, respectively). In contrast, the W^{VI}-based waves are superimposable in shape and intensity. Given that the experimental errors for the peak potential

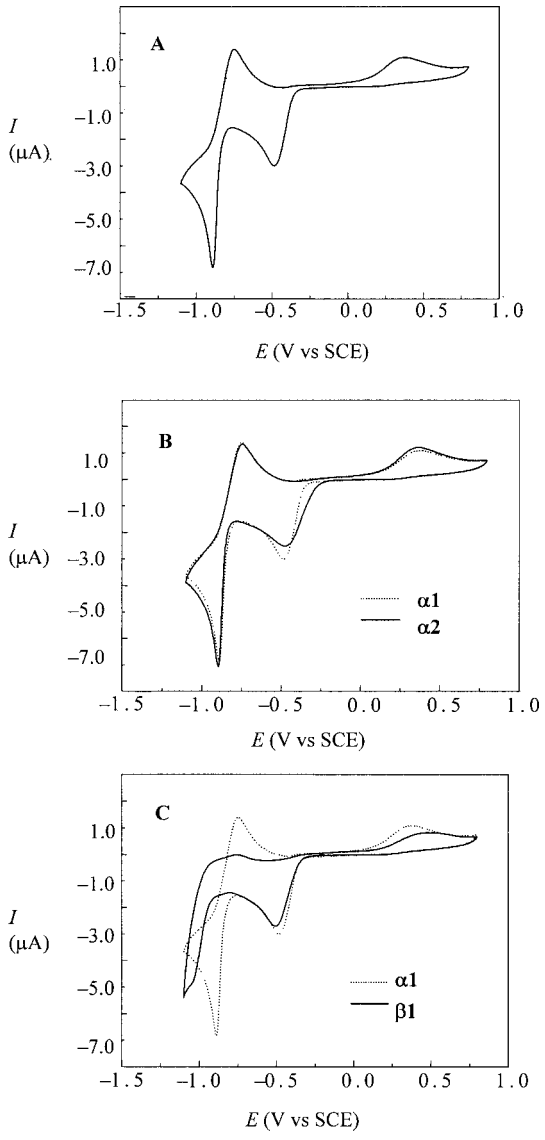

Figure 4. Cyclic voltammograms of **α1**, **α2**, and **β1** in a pH 5 acetate buffer (0.5 M CH_3COONa + CH_3COOH). The pattern has been restricted to the reduction of the Fe^{III} centers and the first W^{VI} reduction process. POM concentration: 0.2 mM; scan rate: 10 mV·s^{-1}; working electrode: glassy carbon; reference electrode: SCE **A:** Cyclic voltammogram of **α1** alone **B:** Cyclic voltammogram of **α1** and **α2** **C:** Cyclic voltammogram of **α1** and **β1**.

measurements of **α2** and **α1** are both ±0.005 V, the difference in the E_{pc} values for the two complexes is quite small. However, the perfect reproducibility of the measurements confirms the order of the peak potentials and suggests their differences are statistically significant. The difference in the peak potentials of **α1** and **α2** could be attributed to the fact that a hydroxo ligand on each Fe^{III} center in **α1** is replaced by an aqua ligand in **α2**. In addition, **α1** has a higher overall negative charge (and slightly higher charge density) than **α2**. Finally, interconversion of the two complexes through protonation equilibria and their co-existence in the same protonation state seems unlikely given the fact that protonation is known to cause the dimer to convert to the monomer.[9]

Figure 4 (C) compares the cyclic voltammograms of **α1** and its Baker–Figgis rotational isomer, **β1** (0.2 mM POM in 0.5 M acetate buffer, pH 5; scan rate 10 $mV \cdot s^{-1}$). Complex **β1** has a negative shift in its peak potentials for both the Fe^{III} and the W^{VI} redox processes. The absolute values of the reduction peak potential differences are 0.022 V and 0.162 V for Fe^{III} and W^{VI}, respectively. To the best of our knowledge, these observations are unprecedented as all previously characterized β-isomers of the unsubstituted Keggin and Wells–Dawson heteropolytungstates are reduced at potentials that are slightly more positive than their corresponding α-isomers.[12] The Fe^{III}-based waves are chemically reversible for both **α1** and **β1**, but **β1** has more pronounced electrochemical irreversibility than **α1**. In addition, the chemical reversibility of the W^{VI}-based wave of **α1** vanishes completely in **β1**. Finally, a small, reversible process observed between the Fe^{III} and W^{VI} waves of **β1** is tentatively attributed to the formation of a small amount of **α1**.

Differences in the electrochemical properties of **α1** and **β1** must be at least partly attributable to the fact that crystallographic studies show these complexes are truly Baker–Figgis rotational isomers. A correlative reason might be traced to differences in the pK_a values of the various protonateable centers in **α1** and **β1**, the latter complex being the more acidic of the two. To probe this further, exhaustive controlled potential electrolysis of the Fe^{III} centers in **β1** was performed using a glassy carbon plate in pH 5 acetate buffer with the potential set at –0.550 V. The current became negligibly small after the consumption of 5.3 electrons per molecule. Cyclic voltammograms (restricted to the Fe^{III}-based redox process) were run before and after electrolysis. When the same glassy carbon plate was used for the initial voltammogram, electrolysis, and the final voltammogram (for a total of three runs), a desorptive oxidation peak and a composite Fe reduction wave appear. This suggests that adsorption and transformation of **β1** has taken place on the surface of the electrode (see Figure S2 in the Supporting Information). Quantitative re-oxidation of the solution to the Fe^{III} state was not possible, as indicated by controlled potential coulometry data (consumption of 2.5 ± 0.1 electrons per molecule). Figure 5 shows the cyclic voltammogram of **β1** before and after the forward and backward electrolysis using a clean carbon plate electrode. The results show that the Fe-wave has become composite and is now located at a more positive potential. Given the fact that this transformation is not observed for **α1**, these observations collectively suggest that **β1** is less stable than **α1** upon the reduction of the Fe^{III} centers.

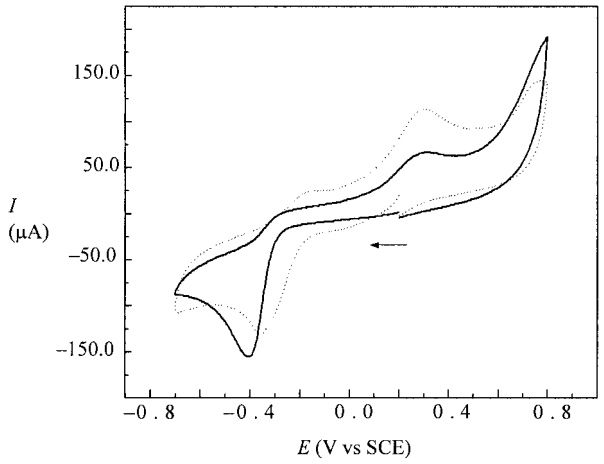

Figure 5. Cyclic voltammograms of **β1** in a pH 5 acetate buffer (0.5 M CH_3COONa + CH_3COOH) before electrolysis of the Fe^{III} centers (solid line) and after exhaustive reduction of the Fe^{III} centers and complete re-oxidation of the resulting solution (dotted line). The pattern has been restricted to the reduction and reoxidation of the Fe^{III} centers only. POM concentration: 0.2 mM; scan rate: 10 $mV \cdot s^{-1}$; working electrode: glassy carbon plate; reference electrode: SCE.

Conclusions

The redox chemistry of three closely related multi-iron silicotungstates have been investigated in order to determine how dimerization and rotational isomerization affects the electrochemical properties of these complexes. In a pH 5 acetate buffer, there is a positive shift in the Fe^{III}-based peak potential upon going from the dimer, $[(\alpha\text{-}Si\text{-}Fe_3W_9(OH)_3O_{34})_2(OH)_3]^{11-}$ (**α1**), to its monomeric derivative $[(\alpha\text{-}Si(FeOH_2)_3W_9(OH)_3O_{34})]^{4-}$ (**α2**). This is due in part to the higher overall charge of the dimer, and it is also partly attributable to differences in the coordination environments of Fe^{III} in the two complexes (i.e. a hydroxo ligand on each Fe^{III} center in **α1** is replaced with an aqua ligand in **α2**, based on BVS calculations on the X-ray crystal structure data). The peak potentials of the Fe^{III}- and W^{VI}-based redox processes of **β1** are both found at more negative values than its rotational isomer **α1**. Exhaustive controlled potential electrolysis studies of the Fe^{III} centers in **β1** collectively suggest that **β1** is less stable than **α1** upon the reduction of the Fe^{III} centers.

Experimental Section

General Methods and Materials: $KNa_3[(\alpha\text{-}Si(FeOH_2)_3W_9(OH)_3O_{34})]$, $K_4Na_7[(\alpha\text{-}SiFe_3W_9(OH)_3O_{34})_2(OH)_3]$, and $Na_9H[\beta\text{-}SiW_9O_{34}]$ were obtained by published procedures[9,13] and purity was confirmed by infrared and UV/Vis spectroscopy and elemental analyses. Elemental analyses of Fe, K, Na, Si, and W were performed by Desert Analytics (Tucson, Arizona). Infrared spectra (2% sample in KBr) were recorded with a Nicolet 510 instrument. The electronic absorption spectra were taken with a Perkin–Elmer Lambda 19 UV/Vis spectrophotometer. Average magnetic susceptibilities were measured with a Johnson-Matthey Model MSB-1 magnetic susceptibility balance as neat powders at 24 °C; the balance was calibrated using $Hg[Co(SCN)_4]$ as a standard. Pascal's constants were used to obtain the final diamagnetic corrections. Differential scanning calorimetric and thermogravimetric data were collected with ISI DSC 550 and TGA 1000 instruments, respectively.

Synthesis of $K_4Na_7[(\beta\text{-}SiFe_3W_9(OH)_3O_{34})_2(OH)_3]\cdot 40H_2O$ (β1): A 0.87 g (2.2 mmol) sample of $Fe(NO_3)_3\cdot 9H_2O$ was dissolved in 30 mL of 0.5 M sodium acetate in an 150 mL beaker. A 2.0 g (0.72 mmol) sample of $Na_9H[\beta\text{-}SiW_9O_{34}]\cdot 18H_2O$[13] was slowly added to the Fe^{III} solution with vigorous stirring. The final pH of

the solution is ca. 6. Any insoluble material that was present was removed by filtration with Celite, and a solution of 0.5 g of KCl dissolved in 5 mL of H_2O was added to the resulting filtrate. Light green, diffraction quality crystals formed at 10 °C in the resulting filtrate after approximately five days (0.43 g, yield 20%). IR (2% KBr pellet, 1200–500 cm^{-1}): $\tilde{\nu}$ = 1129 (w), 991 (w), 960 (m), 883 (s), 811 (w), 770 (w), 724 (m), and 523 (w). Electronic spectroscopic data (400–700 nm, in H_2O): λ (ε, M^{-1} cm^{-1}) = 436 nm (200). Magnetic susceptibility: μ_{eff} = 7.7 μ_B/mol at 295 K. $H_{89}Fe_6K_4Na_7O_{117}Si_2W_{18}$ (5979.5): calcd. Fe 5.60, K 2.62, Na 2.69, OH_2 12.0, Si 0.94, W 55.3; found Fe 5.65, K 2.61, Na 2.64, OH_2 12.0, Si 0.94, W 54.9.

Crystallographic Studies of β1: Single-crystal X-ray crystallographic analysis of **β1** was performed at 100 K with a Bruker D8 SMART APEX CCD sealed tube diffractometer with graphite-monochromated Mo-K_α (0.71073 Å) radiation. Data collection, indexing, and initial cell refinements were carried out using SMART software.[14] Frame integration and final cell refinements were carried out using SAINT software.[15] Final cell parameters were determined from least-squares refinement on 7765 reflections. Absorption corrections were applied using SADABS.[16] The structure was determined using Direct Methods and difference Fourier techniques. No H atoms associated with the water molecules of **β1** were located in the difference Fourier maps. The final R_1 scattering factor and the anomalous dispersion correction were taken from International Tables for X-ray Crystallography.[17] Structure solution, refinement, and generation of publication materials were performed using SHELXTL V6.12 software. Additional details are provided in Table 2, and may also be obtained from the FIZ Karlsruhe, 76344 Eggenstein-Leopoldshafen, Germany, on quoting the depository number CSD-414457.

Table 2. Crystallographic data and structure refinement for **β1**.

Empirical formula	$H_{90.6}Fe_6K_4Na_7O_{117.8}Si_2W_{18}$
Formula mass	5994.04
Space group	Pbcm
Unit cell	a = 12.9709(7) Å
	b = 38.720(2) Å
	c = 21.4221(12) Å
Volume	10758.9(10) $Å^3$
Z	4
Density (calcd.)	3.701 $g\,cm^{-3}$
Temperature	100(2) K
λ	0.71073 Å
μ	2.0272 cm^{-1}
GOF	1.382
Final R_1[a] [$I > 2\sigma(I)$]	0.0848
Final wR_2[b] [$I > 2\sigma(I)$]	0.1674

[a] $R_1 = \Sigma||F_o| - |F_c||/|F_o|$. [b] $wR_2 = \{\Sigma[w(F_o^2 - F_c^2)^2]/\Sigma[w(F_o^2)^2]\}^{0.5}$.

Electrochemical Studies: Cyclic voltammetry studies were performed on 2×10^{-4} M solutions of **α1**, **α2**, or **β1** in a pH 5 acetate (0.5 M CH_3COONa/CH_3COOH) medium, unless otherwise stated. Solutions were de-aerated with Ar for 30 min prior to measurements and kept under positive pressure at all times. The source, mounting, and polishing of the glassy carbon electrodes (GC, Tokai, Japan, 3 mm diameter) have been described in previous work.[18] The counter electrode was a platinum gauze of large surface area. The electrochemical apparatus was a EG and G 273A under computer control (M270 software). All experiments were performed at ambient temperature, and potentials are quoted against a saturated calomel electrode (SCE). Controlled potential coulometry determinations were performed as described for the cyclic voltammetry experiments except that the working electrode used was a 4 cm^2 surface area glassy carbon plate. In addition, after deaeration, Ar was continuously bubbled through the solution to ensure a constant stirring of the mixture. The stability of the complexes in pH 3–7 buffer solutions was evaluated by UV/Vis prior to making any electrochemical measurements. The UV/Vis spectra of 0.016 mM solutions of the POMs are characterized by well-defined charge transfer peaks with a $\lambda_{max.}$ at 259 nm for **α1** and **α2** or 264 nm for **β1**. After 24 h, **α1** shows an 11% decrease in absorbance at pH 4 and is stable between pH 5–7; **β1** is stable between pH 5–7 and shows a 12% decrease in absorbance at pH 4; **α2** is stable at pH 4 and shows a slight shape modification at pH 5.

Supporting Information (see also the footnote on the first page of this article): Figure S1 shows a thermal ellipsoid plot of **β1** with 50% probability surfaces. Figure S2 shows cyclic voltammograms of 0.2 mM solutions of **β1** before and after the exhaustive reduction of the Fe^{III} centers in a pH 5 acetate (0.5 M CH_3COONa/CH_3COOH) buffer.

Acknowledgments

This work was supported by the National Science Foundation (Grant CHE-0236686), CNRS (UMR 8000), and the University Paris-Sud XI.

[1] C. L. Hill, C. M. Prosser-McCartha, *Coord. Chem. Rev.* **1995**, *143*, 407–455.
[2] Recent reviews include: a) R. Neumann, Applications of Polyoxometalates in Homogeneous Catalysis. In *NATO Science Series II: Mathematics, Physics, and Chemistry*; Kluwer Academic Publishers: Dordrecht, **2003**; vol. 98, pp. 327–349; b) I. V. Kozhevnikov, Heterogeneous Catalysis by Heteropoly Compounds. In *NATO Science Series II: Mathematics, Physics, and Chemistry*; Kluwer Academic Publishers: Dordrecht, **2003**; vol. 98, pp. 351–380; c) E. Papaconstantinou, A. Hiskia, Photochemistry and Photocatalysis by Polyoxometalates. In *NATO Science Series II: Mathematics, Physics, and Chemistry*; Kluwer Academic Publishers: Dordrecht, **2003**; vol. 98, pp. 381–416; d) C. L. Hill, Polyoxometalates: Reactivity. In *Comprehensive Coordination Chemistry II: Transition Metal Groups 3–6* (Ed.: A. G. Wedd) Elsevier Science: New York, **2004**; vol. 4, chapter 4.11, pp. 679–759.
[3] Representative work on the synthesis of multi-iron POMs include: a) X. Zhang, Q. Chen, D. C. Duncan, C. Campana, C. L. Hill, *Inorg. Chem.* **1997**, *36*, 4208–4215; b) C. Nozaki, I. Kiyoto, Y. Minai, M. Misono, N. Mizuno, *Inorg. Chem.* **1999**, *38*, 5724–5729; c) X. Zhang, T. M. Anderson, Q. Chen, C. L. Hill, *Inorg. Chem.* **2001**, *40*, 418–419; d) U. Kortz, M. G. Savalieff, B. S. Bassil, B. Keita, L. Nadjo, *Inorg. Chem.* **2002**, *41*, 783–789; e) T. M. Anderson, X. Zhang, K. I. Hardcastle, C. L. Hill, *Inorg. Chem.* **2002**, *41*, 2477–2488; f) I. M. Mbomekalle, B. Keita, L. Nadjo, W. A. Neiwert, L. Zhang, K. I. Hardcastle, C. L. Hill, T. M. Anderson, *Eur. J. Inorg. Chem.* **2003**, 3924–3928.
[4] B. Keita, I. M. Mbomekalle, Y. W. Lu, L. Nadjo, P. Berthet, T. M. Anderson, C. L. Hill, *Eur. J. Inorg. Chem.* **2004**, 3462–3475.
[5] B. Keita, I. M. Mbomekalle, L. Nadjo, T. M. Anderson, C. L. Hill, *Inorg. Chem.* **2004**, *43*, 3257–3263.
[6] R. Contant, M. Abbessi, J. Canny, A. Belhouari, B. Keita, L. Nadjo, *Inorg. Chem.* **1997**, *36*, 4961–4967.
[7] I. M. Mbomekalle, B. Keita, L. Nadjo, P. Berthet, K. I. Hardcastle, C. L. Hill, T. M. Anderson, *Inorg. Chem.* **2003**, *42*, 1163–1169.
[8] L. C. W. Baker, J. S. Figgis, *J. Am. Chem. Soc.* **1970**, *92*, 3794–3797.
[9] T. M. Anderson, W. A. Neiwert, K. I. Hardcastle, C. L. Hill, *Inorg. Chem.* **2004**, *43*, 7353–7358.

[10] J. Liu, F. Ortéga, P. Sethuraman, D. E. Katsoulis, C. E. Costello, M. T. Pope, *J. Chem. Soc., Dalton Trans.* **1992**, 1901–1906.
[11] I. D. Brown, D. Altermatt, *Acta Crystallogr. Sect. B* **1985**, *41*, 244–247.
[12] a) M. T. Pope, *Heteropoly and Isopoly Oxometalates*; Springer-Verlag: Berlin, **1983**; b) M. Sadakane, E. Steckhan, *Chem. Rev.* **1998**, *98*, 219–237 and references cited therein.
[13] A. Tézé, G. Hervé, in *Inorganic Syntheses* (Ed.: A. P. Ginsberg); John Wiley & Sons: New York, **1990**; vol. 27, pp. 85–96.
[14] *SMART*, version 5.628; Bruker AXS, Inc.: Madison, WI, **2003**.
[15] *SAINT*, version 6.36A; Bruker AXS, Inc.: Madison, WI, **2002**.
[16] G. Sheldrick, *SADABS*, version 2.10; University of Göttingen: Göttingen, Germany, **2003**.
[17] *International Table for X-ray Crystallography*; Kynoch Academic Publishers: Dordrecht, The Netherlands, **1992**, vol. C.
[18] B. Keita, F. Girard, L. Nadjo, R. Contant, R. Belghiche, M. Abbessi, *J. Electroanal. Chem.* **2001**, *508*, 70–80.

Received: December 29, 2004

